Desalination and Water Treatment
www.deswater.com

doi: 10.5004/dwt.2017.21393

89 (2017) 258–273
September

Random forest modeling for the kinetic and isotherm study of malachite green adsorption from aqueous environments using zinc sulfide nanoparticle loaded with activated carbon

A. Ansari[a,*], M. Ghaedi[b], A.M. Ghaedi[c], F. Bahari[c], G. Azarian[d], K. Godini[d]

[a]*Faculty of Chemistry, Bu-Ali Sina University, Hamadan 65178-38683, Iran, email: aminansari138@yahoo.com*
[b]*Chemistry Department, Yasouj University, Yasuj 75918-74831, Iran, email: m_ghaedi@mail.yu.ac.ir*
[c]*Chemistry Department, Gachsaran Branch, Islamic Azad University, Gachsaran, Iran,*
emails: abm_ghaedi@yahoo.com (A.M. Ghaedi), baharifarzaneh@yahoo.com (F. Bahari)
[d]*Faculty of Health and Research Center for Health Sciences, Department of Environmental Health Engineering, Hamadan University of Medical Sciences, Hamadan, Iran, Tel./Fax: +988118381641,*
emails: gh_azarian@yahoo.com(G. Azarian), kgoodini@razi.tums.ac.ir (K. Godini)

Received 2 February 2017; Accepted 29 August 2017

ABSTRACT

In this study, a novel zinc sulfide nanoparticle loaded with activated carbon (ZnS-NP-AC) was used to treat hazardous dye malachite green (MG) from aqueous solution. Further, multiple linear regression (MLR) and random forest (RF) were applied to project the performance of the process. Bruner–Emmet–Teller surface area measurement, field emission scanning electron microscope, X-ray diffraction, Barrett–Joyner–Halenda and UV spectrum analyses were utilized to characterize the prepared adsorbent. Over 98% of the dye was removed under optimal conditions: initial pH 7, contact time 30 min, adsorbent dose 0.02 g and initial dye concentration 15 mg L^{-1}. The adsorption efficacy continued to stay unchanged when pH ranged from 2 to 8. It was found that the dye adsorption followed the pseudo-second-order rate equation. To determine the rate-limiting step of the adsorption process, the intraparticle diffusion model was employed. The Langmuir isotherm model fitted the data significantly better and adsorption capacity was 500 mg g^{-1} of the adsorbent. The novel adsorbent investigated in this study can be considered as a suitable alternative for MG removal from aqueous solutions. The optimum tuning variables in the RF model were attained according to n_{tree} = 100, m_{try} = 2, importance = 1 and nPerm = 3. To test data set, the mean squared error (MSE) values of 7.1e–04 and the coefficient of determination (R^2) value of 0.9826 for the RF model and the MSE value of 0.008 and the R^2 value of 0.9091 for the MLR model were achieved. The findings showed that the RF model is a better model than MLR.

Keywords: Zinc sulfide nanoparticles; Random forest; Activated carbon; Adsorption kinetics and isotherm; Malachite green

1. Introduction

Effluents released from different industries such as textile, paper, leather tanning, production, hair colorings and henceforth contain huge quantities of various dyes, which can contaminate the environment and endanger human health [1,2]. For example, malachite green (MG) is widely used for dyeing silk, cotton, leather, paper, as well as making paints and printing inks. It is a toxic dye, which should be treated well before being discharged into the environment [3,4]. Although many dyes have been removed from aqueous environments by using activated carbon, this adsorbent is still expensive. Therefore, the objective of the present study was to extend low-cost adsorbents including natural, agricultural and industrial by-product wastes. In order to treat

* Corresponding author.

dye-laden effluents, adsorption is the most widely applied method owing to its low costs and ease of operation [5,6]. Researchers have studied the potential of many agricultural wastes and by-products of cellulose origin, such as peanut hulls [7,8], maize bran [9], sawdust [10], clay sugar beet pulp [11], crab peel [12], granular kohlrabi peel [13], raw barley straw [14], eggshell [15], aquaculture shell powders, etc. [16] for removal of dyes from aqueous solutions. Also, unconventional adsorbents like wood [17,18], silica [19], clay and activated clay [20,21], agricultural residues [22] and henceforth have been taken into account. Thus, it is very important to investigate the adsorption potential of local resources that have high adsorption capacity. The size, surface structure and high surface areas (reactive atom or functional groups) are the main factors of nanoparticle materials for the strong chemisorption of many chemical compounds [23–25].

Since adsorption is a complex and non-linear process, the modeling of it is very important. Hence, to solve a series challenges with engineering applications such as adsorption, various intelligence systems like artificial neural networks [1–4], adaptive neuro-fuzzy inference system [5,6] and support vector machine [26] have widely been employed lately. Random forest (RF) is another non-linear and potent technique, which is relatively novel, used in the classification and regression problems. To our best knowledge, the application of RF in regression type of adsorption applications has been investigated only by a few researchers [8]. Besides, the aim of this research was to compare the results of the RF model with those obtained through a conventional multiple linear regression (MLR) to project the removal (%) of the dye from aqueous media via zinc sulfide nanoparticles loaded with activated carbon. Further, a green method was used for the synthesis of the ZnS nanoparticles. And, the nanoparticles were characterized by a few instrumental methods including X-ray diffraction (XRD), field emission scanning electron microscope (FESEM), Bruner–Emmet–Teller (BET), Barrett–Joyner–Halenda (BJH) and UV spectrum. High amounts of this dye can be removed by means of the prepared adsorbent having a high adsorption capacity at a very short contact time. Furthermore, to study the adsorption mechanisms, the kinetics and equilibrium data were analyzed and diverse models were employed to fit the experimental data.

2. Experimental

2.1. Instruments and reagents

The dye, MG, C.I. Basic Green 4, C.I. Classification Number 42,000, chemical formula = $C_{52}H_{54}N_4O_{12}$, molecular weight = 927.00, λ_{max} = 617 nm (measured value) was detected by a UV–Vis spectrophotometer (DR 5000 model; Hach, USA). Fig. 1 shows the chemical structure of MG. All chemicals used (MG, NaOH, KCl and HCl) were of the highest quality and obtained from Merck (Darmstadt, Germany). The stock solution (1,000 mg L^{-1}) of the dye was prepared through dissolving a sufficient content of the solid dye in double distilled water, and then the working concentrations were prepared daily. The different pH values were detected by using a pH/ion meter (Metrohm, Switzerland, Swiss) and the MG concentrations were measured by means of a UV–Vis spectrophotometer (DR 5000 model; Hach, USA) at the wavelength of 617 nm. XRD patterns were recorded by an automated (Philips, Netherland) X'Pert X-ray diffractometer (40 kV and 30 mA) for 2θ values over 10°–80°. The laser light scattering (Zetasizer Nano series, Malvern Instruments Co., Malvern, UK) was used to determine the particle size and size distribution of the ZnS nanoparticles. The FESEM (Hitachi S-4160, Japan) was studied according to conditions previously reported in literature by instruments reported elsewhere. A BET surface analyzer (Quantachrome NOVA 2000, USA) was utilized for the estimation of adsorption–desorption isotherm at 77 K. Before each run, all samples were degassed using helium purging at 553 K for 3 h.

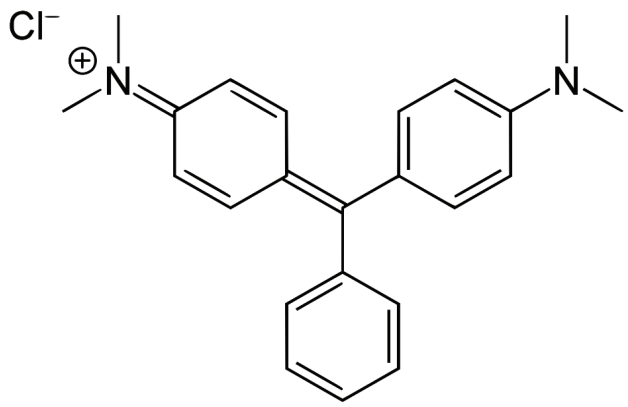

Fig. 1. Chemical structure of malachite green.

2.2. Measurement of dye uptake

Hence, to determine dye concentrations, the absorbance of the test samples at the maximum absorbent wavelength of MG (λ_{max}: 617 nm) was detected via a UV/Vis spectrophotometer (DR-5000 model, Hach, USA). The efficiency of MG removal was determined at different time intervals ranging from 0.5 to 35 min for ZnS-NP-AC. Moreover, the pH values (2–8) were adjusted to evaluate the influence of initial pH, by contacting 50 mL of the solution containing 15 mg L^{-1} of initial dye concentration with 0.01 g of ZnS-NP-AC for 35 min. In addition, to attain adsorption isotherms, all experiments were conducted at the initial MG contents from 5 to 30 mg L^{-1} for ZnS-NP-AC. The removal efficiency (%) of MG was calculated by Eq. (1):

$$\%\ \text{MG removal} = \frac{(C_0 - C_t)}{C_0} \times 100 \tag{1}$$

where C_0 (mg L^{-1}) and C_t (mg L^{-1}) are, respectively, the contents of the dye at before and after time t. The adsorbed MG amount (q_e, mg g^{-1}) was calculated by the mass balance equation as follows:

$$q_e = \frac{(C_0 - C_e)V}{W} \tag{2}$$

where C_0 (mg L^{-1}) and C_e (mg L^{-1}) are the initial and equilibrium dye concentrations in aqueous solution, respectively, V (L) is the volume of the solution and W (g) is the amount of the adsorbent.

2.3. Preparation of ZnS nanoparticles

The ZnS nanoparticles were synthesized in accordance with the reaction of zinc acetate [$Zn(CH_3COO)_2{\cdot}2H_2O$] with thioacetamide ($CH_3CSNH_2$) in oxygen-free water under nitrogen. According to the conventional synthesis, 10 mL of the freshly prepared thioacetamide solution (0.1 M) was added to 50 mL of $Zn(CH_3COO)_2{\cdot}2H_2O$ and trisodium citrate at pH of 6.0 under intensive stirring, while the actual contents of thioacetamide, zinc acetate and trisodium citrate presented were 0.5, 1 and 5 mM, respectively. The prepared mixture was heated to 40°C, at which the growth of the citrate-stabilized ZnS nanoparticles started gradually; the solution changed milky white after nearly 10 min illustrating the initial formation of the ZnS nanoparticles. And, the color of the reaction solution got milky white mixed with light yellow after the mixture was remained at 40°C for 6 h. Then, the attained ZnS nanoparticles were separated from the reaction mixture by means of centrifugation and washed a few times with ultrapure water and ethanol for removing the impurities and trisodium citrate. Finally, the prepared nanoparticles were dried in a vacuum oven (ca. 0.1 MPa) for 6 h before being characterized.

2.4. Random forest

RF is a powerful method, accomplished to boost the classification and the regression tree method by containing hundreds of unpruned decision trees [7]. The goal of the RF is to decline the correlation between the individual trees by bootstrapping and randomized variable selection method, leading to lessened variance when the trees are aggregated. The RF algorithm needs the tuning variables: n_{tree}, regression trees grown number based on a bootstrap sample of the original data set (the default value is 500 trees) and m_{try}, the number of different predictors to try at each node (the default value is one-third of the total number of the variables) and nodesize, the minimum size of terminal nodes. Larger numbers of nodesize cause smaller trees (the default values are 1 and 5 for classification and regression, respectively). Briefly, the RF regression model performs as follows (see reference [7]):

- Start with a set of data, including input and output.
- Selection of the original samples (about 67%) will be chosen in a bootstrap sample (called the in-bag samples) and about 33% of them will be left out (called the out-of-bag [OOB] samples). Bootstrap is a statistical terminology for sampling with replacement. In this research, 70% and 30% of the original samples were chosen for OOB and in-bag samples, respectively.
- Selection of the m_{try} recommended that the value of the default (default is floor (sqrt (size (X, 2)) and X is data matrix), half of them and twice they will be implemented and then the best of value among them will be selected. The small value of tuning parameter m_{try} will be prevented overfitting.
- Choices of the n_{tree} and the making of a tree according to the in-bag and the m_{try} variables were selected. Hence, to attain an optimum of the n_{tree}, the trees must be built until the error no longer decreases.

The experimental data set are randomly divided into the training set and the testing set. Among 360 data, 252 are considered as training data and 108 as testing data. All computations were conducted with the Random Forest-Matlab package invented by Abhishek Jaiantilal (https://github.com/jrderuiter/randomforest-matlab). The inputs include concentration (mg L^{-1}), the amount of adsorbent (g) and contact time (min). The output is the removal percentage. Inputs and outputs are normalized between 0.1 and 0.9 to avoid numerical overflows owing to very large or very small weights. The normalization equation applied is as follows:

$$y = (x_i - \frac{x_{\min}}{x_{\max}} - x_{\min}) \times 0.8 + 0.1 \tag{3}$$

where y is the normalized value of x_i. The x_{max} and x_{min} are, respectively, the maximum and minimum values of x_i. In order to investigate the efficiency of the RF model, variables of mean squared error (MSE) and coefficient of determination (R^2) were employed. The equations of the MSE and the R^2 are as follows:

$$\mathrm{MSE} = \frac{1}{N}\sum_{i=1}^{N}\left(\left|y_{\mathrm{prd,i}} - y_{\mathrm{exp,i}}\right|\right)^2 \tag{4}$$

$$R^2 = 1 - \frac{\sum_{i=1}^{N}\left(y_{\mathrm{prd},i} - y_{\mathrm{exp},i}\right)}{\sum_{i=1}^{N}\left(y_{\mathrm{prd},i} - y_m\right)} \tag{5}$$

where $y_{prd,i}$ was the predicted value of the RF model, $y_{exp,i}$ was the experimental value, N was the number of the data and y_m was the average of the experimental value.

2.5. Multiple linear regression

MLR models are often applied to predict more than one predictor variable in various studies to model the impact of predictor variables on the dependent variable. The following mathematical equation shows the MLR model:

$$Y = b_0 + b_i X_i + b_2 X_2 + \ldots + b_n X_n \tag{6}$$

where Y is the predicted value by the MLR model, b_i ($i = 0, \ldots, n$) are the regression coefficients and X_i ($i = 1, \ldots, n$) are the predictor variables (inputs). In addition of the different objectives of the MLR model, it can be easily used in adsorption process to measure the cumulative impact of several predictor variables, including contact time, adsorbent dosage and dye concentration, on a dependent variable (removal (%)). In this research, SPSS 19 statistical program was applied to construct the MLR model.

3. Results and discussion

3.1. Characterization of adsorbent

Absorption spectra measurements were continued to the much longer times than 6 h (Fig. 2). The solution of the ZnS nanoparticles illustrates a well-resolved absorption maximum of the first electronic transition presenting a sufficiently narrow size distribution of the ZnS nanoparticles, which

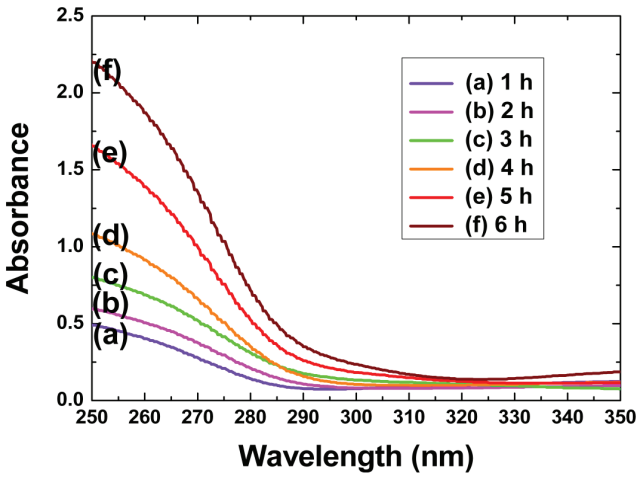

Fig. 2. Evolution of absorption spectra of the ZnS nanocrystals taken at 1 h intervals by following the initiation of the reaction for the first 6 h.

shifts to the shorter wavelengths with reducing the size of the nanoparticles as a consequence of the quantum confinement. As exhibited in Fig. 2, the citrate-stabilized ZnS nanoparticles have absorption edges ranging from 290 to 320 nm (4.26–3.86 eV). From the absorption spectra, the energy band gap of the ZnS nanoparticles was attained by Eq. (7) [5]:

$$(\alpha h\upsilon)^2 = A(E_g - h\upsilon) \tag{7}$$

where E_g presents the band gap of the nanoparticles and A is a characteristic constant. A typical graph of $(\alpha h\nu)^2$ against energy ($h\nu$) for the ZnS nanoparticles is plotted. The energy band gap was acquired via extrapolating the linear portion of the respective curve to $(\alpha h\nu)^2 = 0$. The straight-line property of the curve displayed that the ZnS nanoparticles have the direct band gap ranging from 4.26 to 3.86 eV, while the bulk material has a band gap of 3.67 eV [27]. The XRD pattern attained from the powdered ZnS nanoparticles synthesized at room temperature has been shown in Fig. 3. The standard XRD pattern for ZnS (Joint Committee on Powder Diffraction Standards, JCPDS card No. 05-0566) was specified at the bottom of Fig. 3. The three broad peaks observed in the diffractogram at around 28.56°, 47.43° and 56.25° illustrate a cubic lattice structure of ZnS (β-ZnS phase). These peaks can be attributed to the planes (111), (220) and (311), respectively, of the cubic phase [8]. In addition, diffracted peaks owing to ZnO or $Zn(OH)_2$ in the XRD pattern were not seen in this study. Fig. 4(a) shows diameter size distribution for the ZnS nanoparticles, which is determined by the laser light scattering. The FESEM image of the ZnS nanoparticles is shown in Fig. 4(b), which reveals that the ZnS nanoparticles are semicubical in shape and quite uniform in size distribution. The particle size measured directly from this FESEM image agrees with that determined by the laser light scattering. The particle surface becomes much smoother than that of the original particle following dye adsorption. Designation of specific surface area by N_2/77 K adsorption isotherms was assumed to estimate the surface area in micropores within pore sizes of material [28]. Specific surface area

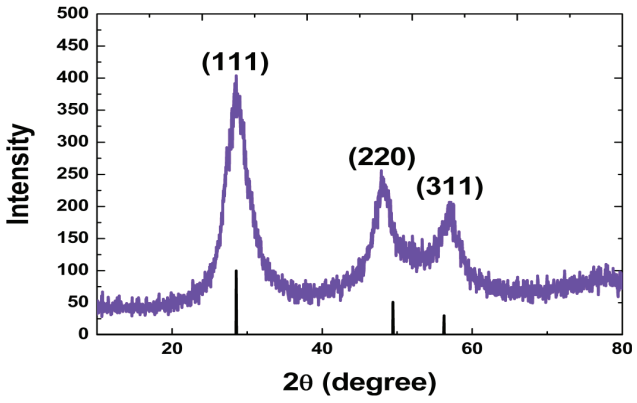

Fig. 3. X-ray diffraction (XRD) pattern of the citrate-stabilized ZnS nanocrystals.

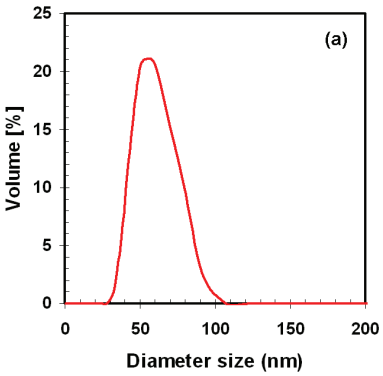

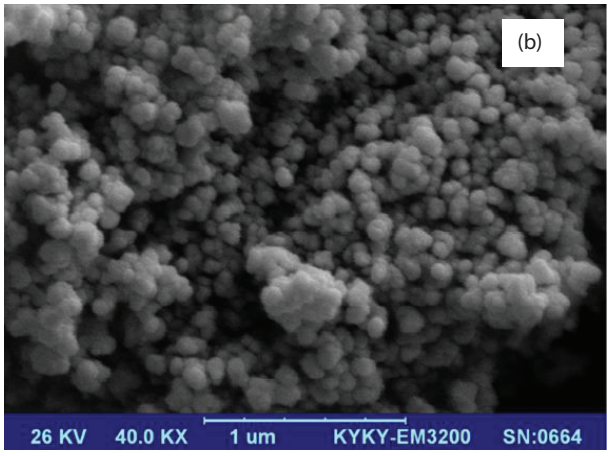

Fig. 4. (a) Histogram of the ZnS nanoparticles size distribution. (b) FESEM image of the ZnS nanoparticles.

is described as the available area of adsorbent surface per unit mass of material. In BET N_2 adsorption/desorption isotherm method, the interference by the surrounding phase is especially problematic as vacuum treatment modifies the entire surface before N_2 adsorption [29]. Based on Fig. 7(a) and Table 1 for nanoparticles ZnS unloaded, the N_2 adsorption isotherm with a hysteresis loop (between p/p_0 = 0.4 and 0.8) is characteristic of a "type IV" isotherm, which is typical of mesoporous material. Also, the pore-size distribution calculated by the BJH method shows an average pore diameter

Table 1
Summary report of ZnS-loaded and unloaded AC

Summary report	ZnS-NP-AC	ZnS-NP unloaded
Surface area		
BET surface area	1,316.16 $m^2 g^{-1}$	603.0782 $m^2 g^{-1}$
Langmuir surface area	1,804.76 $m^2 g^{-1}$	810.1988 $m^2 g^{-1}$
BJH adsorption cumulative surface area of pores between 17.000 and 3,000.000 Å width	129.25 $m^2 g^{-1}$	188.955 $m^2 g^{-1}$
BJH desorption cumulative surface area of pores between 17.000 and 3,000.000 Å width	150.13 $m^2 g^{-1}$	226.9081 $m^2 g^{-1}$
Pore volume		
Single point adsorption total pore volume of pores <1,256.713 Å width at p/p_0 = 0.985304522	0.66 $cm^3 g^{-1}$	0.474262 $cm^3 g^{-1}$
t-Plot micropore volume	0.20 $cm^3 g^{-1}$	0.153036 $cm^3 g^{-1}$
BJH adsorption cumulative volume of pores between 17.000 and 3,000.000 Å width	0.12 $cm^3 g^{-1}$	0.288403 $cm^3 g^{-1}$
BJH desorption cumulative volume of pores between 17.000 and 3,000.000 Å width	0.13 $cm^3 g^{-1}$	0.301245 $cm^3 g^{-1}$
Pore size		
Adsorption average pore width (4 V/A by BET)	20.00 Å	31.4561 Å
BJH adsorption average pore width (4 V/A)	37.17 Å	61.052 Å
BJH desorption average pore width (4 V/A)	34.26 Å	53.104 Å
Nanoparticle size		
Average particle size	45.59 Å	99.490 Å

of 61.052 Å (rp = 30.5 Å). In addition, the BET specific surface area measured from the N_2 isotherms is 603.0782 $m^2 g^{-1}$. However, Fig. 7(b) for ZnS-NP-AC indicated the N_2 adsorption isotherm with a characteristic of a "type I" isotherm, which is typical of microporous material (type of Langmuir). Also, the pore-size distribution calculated by the BJH method for ZnS-NP-AC shows an average pore diameter of 20.0002 Å (rp = 10.0 Å) and the surface area of ZnS-NP-AC was found to be 1,316 $m^2 g^{-1}$. Table 1 and Figs. 5–7 show that adsorbent possessed appreciable narrow microporosity [30].

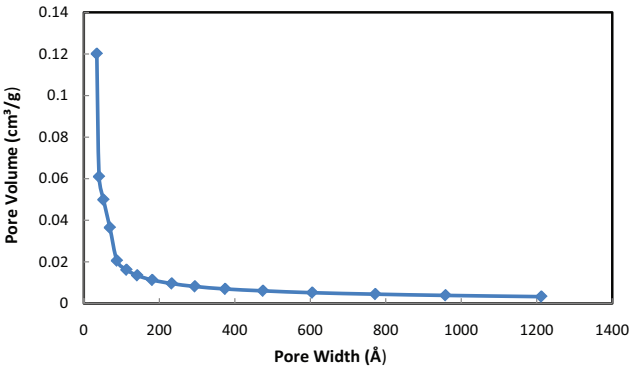

Fig. 5. BJH adsorption cumulative pore volume (larger) Halsey:-Faas correction.

3.2. The effect of pH on dye removal

In wastewater treatment through adsorption, pH is one of the most important factors affecting adsorbent capacity. Fig. 8 shows the impact of pH on MG removal by ZnS-NP-AC. The removal efficiency of MG enhanced from 20% to 70% for 0.01 g and 25% to 80% for 0.015 g of the adsorbent when there was an increase in pH between 2 and 4. At pH values over 6, the removal efficiency went up gradually until it reached a stable amount. It should be noted that the highest removal efficiency was achieved at the pH of 7 and then it started to decrease. It has been claimed that an increase in dye uptake is dependent on the dye structure and the characteristics of adsorbent surface [31]. In acidic conditions, the process apparently shows the protonation of MG, but, when there is an increase in pH, the dye becomes more and more deprotonated. At low pHs, it is possible that the surface of ZnS-NP-AC is positively charged, resulting in a decrease in decolorization [31]. Of course, at pHs over 5, a significant change was not observed in polarity as dye removal increased monotonically with pH. Low pHs, particularly values under 4, were not suitable for the removal of MG via ZnS-NP-AC. When pH is lessened, the number of negatively charged adsorbent sites declines and positively charged sites increases; which this condition is not suitable for the uptake of positively charged MG cations due to the electrostatic repulsion. The same behavior for MG onto the adsorbent has been presented as well as for the removal of a basic dye from aqueous solutions by spent tea leaves [32].

3.3. Effect of contact time

Some experiments were performed to study the effect of contact time (ranging from 0.5 to 35 min) on MG adsorption;

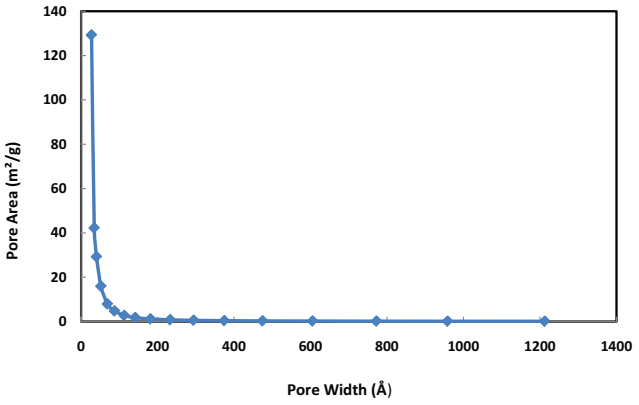

Fig. 6. BJH adsorption cumulative pore area (larger) Halsey:Faas correction.

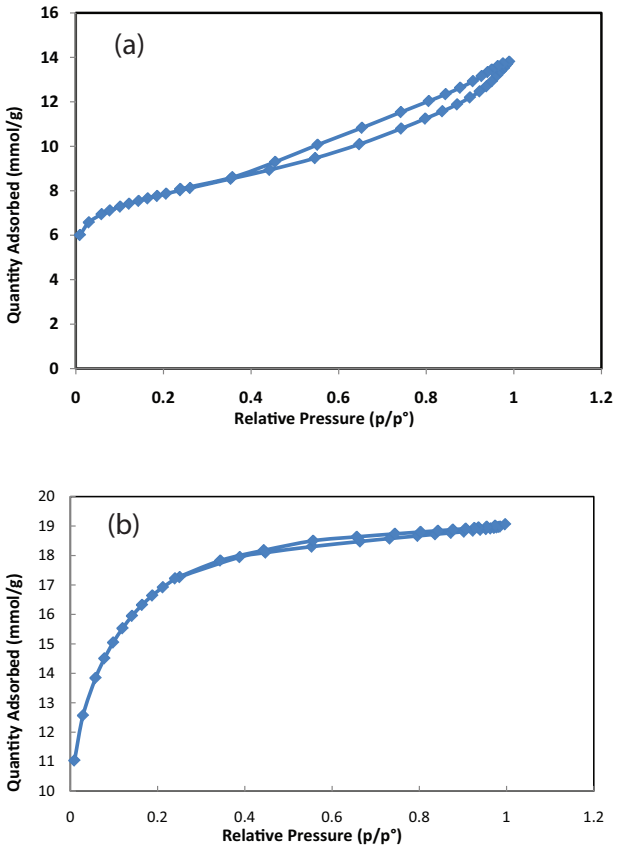

Fig. 7. (a) Isotherm linear plot for ZnS-NP unloaded AC. (b) Isotherm linear plot for ZnS-NP-AC.

Fig. 9 shows the obtained information. Apparently, an increase in contact time led to an increase in removal efficiency of MG at initial content of 15 mg L^{-1} of the dye 0.005–0.02 g of ZnS-NP-AC and pH of 7.0. At the beginning of the reaction, there are many unoccupied sites on the positively charged surface of the adsorbent causing adsorption rate to rise sharply. This adsorbent through soft border line, zinc and sulfide atom or varied functional groups of AC, binds with the MG molecules. It was found that the contact time required for

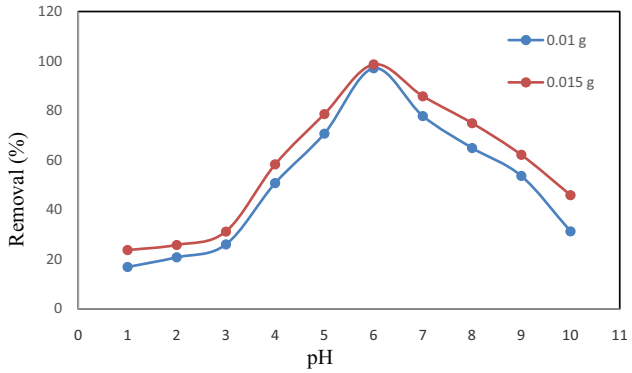

Fig. 8. Effect of solution pH on adsorption of MG (15 mg L^{-1}) onto ZnS-NP-AC (0.01 and 0.015 g) at room temperature (27°C ± 2°C), agitation speed 400 rpm for the maximum contact time required to reach the equilibrium (35 min).

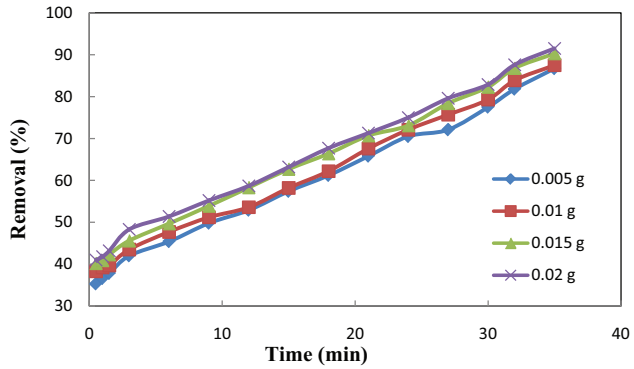

Fig. 9. Effect of contact time (0.5–35 min) on the removal of different concentrations of MG in 0.005–0.02 g of ZnS-NP-AC at pH 7.0 and 15 mg L^{-1} initial MG concentration.

achieving equilibrium was approximately 25 min and at this time the highest decolorization was reached. It should be noted that the low pore-size distribution and diameter are the disadvantages of the suggested adsorbent making it unsuitable for pore diffusion of the large molecules of the dye; and, adsorption takes a short time (attributed to only surface adsorption to the exterior surface of the adsorbent) [28,29].

3.4. Effect of adsorbent dosage

Adsorbent dosage plays a basic role in adsorption because the capacity of the adsorbent for a certain amount of dyestuff is determined by this variable [33]. Fig. 10 presents the impact of different adsorbent dosages on MG degradation. As can be clearly seen, decolorization enhanced quickly when the dose was raised to 0.02, and, in the case of doses higher than this value, the decolorization leveled off. When there are higher doses of the adsorbent, the adsorbent surface area and availability of more active adsorption sites on the ZnS-NP-AC surface increase. On the other hand, on account of aggregation of the adsorbent particles, the adsorbed amount of dye per unit mass of the adsorbent declined with an increase in the adsorbent dosage.

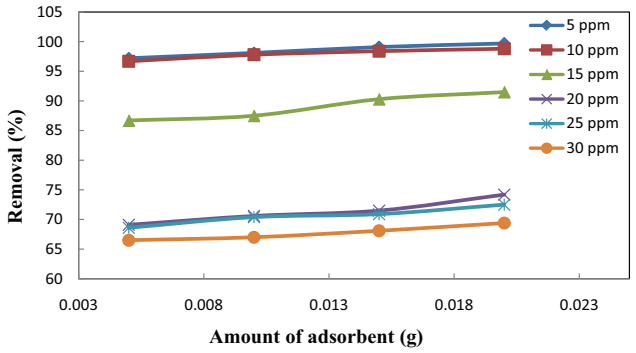

Fig. 10. Effect of adsorbent dosage on MG removal in the range of 0.005–0.02 g at various initial MG concentrations (5–30 mg L^{-1}), contact time 35 min, pH 7.0, agitation speed 400 rpm, temperature 27°C ± 2°C.

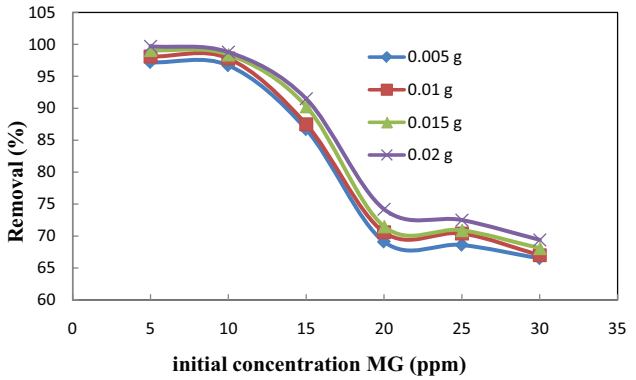

Fig. 11. Effect of initial concentration (5–30 mg L^{-1}) of MG removal at 0.005–0.02 g adsorbent onto ZnS-NP-AC, 35 min contact time, pH 7.0, agitation speed 400 rpm, temperature 27°C ± 2°C.

3.5. Effect of initial MG concentration

Initial concentration of dyes plays an important role in the contact time required to achieve equilibrium [28–30]. Fig. 11 shows the impact of contact time on MG adsorption onto ZnS-NP-AC at some concentrations of MG ranging from 5 to 30 mg L^{-1}. When there was a decrease in MG content, the absolute amount of adsorbed MG at the equilibrium condition declined. Higher contents of the adsorbate may result in the more diffusion from the adsorbent surface into the micropores. The highest amount of MG adsorption onto ZnS-NP-AC was reached within 30 min for 0.02 g of ZnS-NP-AC. Raising concentration gradient, acting as the increasing driving force, results in an increase in equilibrium sorption until sorbent saturation is attained [34]. Although the adsorption capacity went up at the equilibrium, a downward trend was seen in adsorption as initial MG content was raised between 5 and 30 mg L^{-1}. The quicker uptake of MG molecules is traceable to solute transfer, as there are only sorbate and sorbent interactions with negligible interference from solute–solute interactions. Thus, at higher initial contents of MG, the amount of adsorption was more and when the mass transfer driving force increased, the uptake of MG declined [24,25,35].

3.6. Isotherm analysis

The equilibrium sorption isotherm is required to design a profitable sorption system and to study the capacity of the adsorbent. Also, a follow-up of adsorption study makes researcher to obtain beneficial information on the characteristics and affinity of the adsorbent surface toward each adsorbate molecule. Equilibrium relationships exhibit the ratio between adsorbed and remained adsorbates in solution at a fixed temperature that describes the nature of the adsorbate–adsorbent interaction. In order to design an applicable experimental equation, which is appropriate for the interpretation of gained information, the analysis of equilibrium data with theoretical or empirical equations is entirely essential [36].

3.6.1. Langmuir isotherm

The theoretical Langmuir isotherm is valid for adsorption of solute from a liquid solution as monolayer adsorption on a finite number of identical surface sites with uniform energies of adsorption onto the surface without transmigration of the adsorbate in the surface plane [37].

$$\frac{C_e}{q_e} = \frac{1}{K_a Q_m} + \frac{C_e}{Q_m} \tag{8}$$

A popular procedure is used to calculate the highest adsorption capacity that accords to complete monolayer coverage on the surface of the adsorbent. A plot of C_e/Q_e vs. C_e at various contents of ZnS-NP-AC ranges between 0.005 and 0.02 g presents a straight line with a slope of $1/Q_m$ and intercept equal to $1/K_a Q_m$. This line has been depicted at various conditions (ZnS-NP-AC concentration) and Table 2 presents the calculated constants of these model parameters. Strong positive proof on the fitness of equilibrium data of the adsorption of MG from the Langmuir model is illustrated owing to the high correlation coefficients (R^2 = 0.9985) and high maximum monolayer capacity (500–100 mg g^{-1} using 0.005–0.02 g adsorbent).

3.6.2. Freundlich isotherm

The Freundlich isotherm model [38] is applicable for non-ideal heterogeneous sorption with the logarithmic decrease in the enthalpy of adsorption with a rise in the fraction of occupied sites:

$$\ln q_e = \ln K_f + (1/n) \ln C_e \tag{9}$$

where constants such as K_f shows information on the bonding energy and known as the adsorption or distribution coefficient and represents the quantity of MG dye adsorbed onto the ZnS-NP-AC adsorbent. $1/n$ presents the adsorption intensity of MG dye onto the adsorbent (surface heterogeneity). The value closer to zero by rising heterogeneous nature of surface ($1/n < 1$) is indicative of a normal Langmuir isotherm while $1/n$ above 1 shows bimechanism and cooperative adsorption. Plotting $\ln(q_e)$ vs. $\ln(C_e)$ was used to estimate the applicability of the Freundlich adsorption isotherm; Table 2 gives the respective values for these model constants at various contents of the adsorbent. It was found that, in comparison with the Langmuir model, the Freundlich model had

Table 2
Isotherm constants of MG adsorption onto ZnS-NP-AC at pH 7, contact time 35 min, concentration MG 5–30 mg L^{-1}, adsorbent dose 0.005–0.02 g and room temperature

Adsorbent (g)						
Isotherm	Equation	Parameters	0.005	0.01	0.015	0.02
Langmuir	$C_e/q_e = 1/K_aQ_m + C_e/Q_m$	Q_m (mg g^{-1})	500	200	142.85	100
		K_a (L mg^{-1})	1	1.666	2.333	2.5
		RL	0.14–0.03	0.13–0.03	0.12–0.03	0.11–0.02
		X^2	195.505	89.438	055.017	35.764
		R^2	0.9985	0.9856	0.9957	0.9964
Freundlich	$\ln q_e = \ln K_f + (1/n)\ln C_e$	$1/n$	0.256	0.241	0.215	0.186
		K_f (L mg^{-1})	202.147	108.310	78.022	63.688
		X^2	216.651	103.182	61.466	40.101
		R^2	0.888	0.877	0.906	0.956
Temkin	$q_e = B_1 \ln K_T + B_1 \ln C_e$	B_1	56.64	26.13	15.62	10.12
		K_T (L mg^{-1})	54.108	100.987	251.640	987.325
		X^2	227.729	109.038	65.634	45.018
		R^2	0.899	0.895	0.908	0.924
Dubinin and Radushkevich	$\ln q_e = \ln Q_s - B\varepsilon^2$	Q_s (mg g^{-1})	285.145	142.879	91.652	71.736
		B	2e–07	9e–08	2e–08	1e–08
		E (kJ mol^{-1}) = $\frac{1}{\sqrt{2B}}$	3,571.428	4,098.360	5,000	7,462.686
		X^2	1,374.898	716.766	529.322	337.998
		R^2	0.920	0.913	0.922	0.890

lower performance because of the correlation coefficients (0.877–0.956) and higher error value of this model.

3.6.3. Temkin isotherm

Judgment for the ability of each model for the exhibition of method applicability for an explanation of experimental data is according to R^2 value and lower values concern to error analysis. Although the Langmuir and even Freundlich models have reasonable and acceptable R^2 value, the applicability of other models like the Temkin model has widely been employed in the following linear form [39–43]: the Temkin isotherm (Eq. (10)) can be simplified to the following equation:

$$q_e = B_l \ln K_T + B_l \ln C_e \tag{10}$$

where $B = (RT)/b$ is an affiliate to the heat of adsorption, T is the absolute temperature in Kelvin and R is the universal gas constant (8.314 J mol^{-1} K^{-1}) [44,45]. The data taken from the adsorption process were analyzed based on the linear form of the Temkin isotherm (Eq. (10)). It was found that this model is effectively capable of fitting the adsorption of the dye onto ZnS-NP-AC. Table 2 presents a breakdown of the linear isotherm constants and coefficients of MG adsorption. When the dosage of ZnS-NP-AC was raised between 0.02 and 0.005 g, the heat of MG adsorption onto ZnS-NP-AC went up between 10.12 and 56.64 kJ mol^{-1}. It should be noted that the Temkin model is applicable for MG adsorption onto ZnS-NP-AC, because its correlation coefficients (R^2 = 0. 924) were comparable with those obtained for the Langmuir and Freundlich equations. However, since the X^2 value is significant, the Langmuir model is the most applicable.

3.6.4. Dubinin–Radushkevich isotherm

Furthermore, to estimate the porosity, free energy and adsorbent properties, the D–R model was employed [41,42]. The D–R isotherm does not assume a homogeneous surface or constant adsorption potential. The D–R model has commonly been used in Eq. (11) and its linear form can be shown in Eq. (12):

$$q_e = Q_{s,\exp}(-B\varepsilon^2) \tag{11}$$

$$\ln q_e = \ln Q_s - B\varepsilon^2 \tag{12}$$

where B is a constant related to the adsorption energy, Q_s is the theoretical saturation capacity and ε is the Polanyi potential, calculated from Eq. (13).

$$\varepsilon = RT \ln\left(1 + \frac{1}{C_e}\right) \tag{13}$$

The slope of the plot of $\ln q_e$ vs. ε^2 gives B ($mol^2\,kJ^{-2}$), and the intercept yields the adsorption capacity, Q_s (mg g^{-1}). In the present study, Eq. (14) was used to calculate the mean free energy of adsorption (E), for transfer of 1 mol of target from infinity in solution to the surface of the solid [43].

$$E = \frac{1}{\sqrt{2B}} \tag{14}$$

Table 2 presents the calculated values of the D–R parameters. The model saturation adsorption capacity at optimum conditions, using a different dose of adsorbent, was in the range of 285.14–71.7 mg g^{-1}, respectively, and has good agreement with the respective Langmuir value. The values of E calculated by using Eq. (14) are 3.5–7.4 kJ mol^{-1} corresponding to physicosorption process plays a basic role in MG adsorption onto ZnS-NP-AC. Error analysis (χ^2) is another standout factor for the evaluation of the applicability of each model. The non-linear chi-square test statistic (χ^2) [44] (the best-fit isotherm) is based on the following equation:

$$\chi^2 = \frac{\sum\left(q_{e,\exp} - q_{e,\text{cal}}\right)^2}{q_{e,\text{cal}}} \tag{15}$$

where $q_{e,\exp}$ and $q_{e,\text{cal}}$ are experimental and calculated adsorption capacity values, respectively. The good agreement of the data acquired by each model to the experimental data caused, χ^2 will be a smaller number and non-applicability of each model makes possible a larger χ^2 value. The obtained non-linear value, which is higher than the r^2 value and smaller than the χ^2 value of the Langmuir isotherm compared with the similar value of other applied model, confirms the high efficiency of the Langmuir isotherm to represent the experimental data in all conditions. The lower correlation coefficient (R^2) of the Freundlich model, in comparison with the Langmuir model, suggests that the removal process was better modeled by monolayer compared with multilayer adsorption. In order to confirm this result, the favorable or unfavorable MG adsorption onto the adsorbent in Langmuir model is judged by calculation of the separation factor (RL) for evaluation of the adsorption capacity [35].

$$RL = \frac{1}{\left(1 + K_a C_0\right)} \tag{16}$$

where K_a (L mg^{-1}) is the Langmuir constant and C_0 (mg L^{-1}) is the initial concentration. The adsorption can be considered as a favorable process if RL is between 0 and 1. In this study, since the RL value is lower than 1, the adsorption process is favorable and the Langmuir model showed a good fit to the experimental data in all adsorbent dosages and initial MG concentrations. On the other hand, a rise in initial MG concentration and the adsorbent dosage causes the RL value to increase, thereby increasing the tendency of MG for adsorption onto ZnS-NP-AC.

3.7. Adsorption kinetics

The kinetic survey shows the rate and the mechanism of the adsorption process. Two different mechanisms described dye adsorption on a solid surface: (i) an initial quick binding of molecules of the dye on the adsorbent surface followed by (ii) relatively slow intraparticle diffusion.

3.7.1. Pseudo-first-order kinetic model

The pseudo-first-order kinetic model [10] assumes that the rate of change of solute uptake with time is directly proportional to the difference in saturation concentration and the amount of solid uptake to time. In most cases the adsorption reaction preceded by diffusion through a boundary, the kinetics follows the pseudo-first-order rate equation. The rate constant of adsorption is described as a first-order rate expression as follows:

$$\frac{dq_t}{dt} = k_1(q_e - q_t) \tag{17}$$

where q_e and q_t are the amounts of dye adsorbed (mg g^{-1}) at contact time t (min) and equilibrium, respectively, and k_1 is the pseudo-first-order rate constant (min^{-1}). The rate law for a pseudo-first-order reaction results in Eq. (18) after integrating and rearranging Eq. (17) [45]:

$$\log(q_e - q_t) = \log q_e - \frac{k_1}{2.303}t \tag{18}$$

The plot $\log(q_e - q_t)$ vs. t should give a straight line with a slope of k_1 and intercept allowing the calculation of adsorption rate constant and equilibrium adsorption capacity. It may be seen that the experimental data point does not fit a straight line. It may be attributed to the stirring speed employed in the current research (400 rpm) decreasing the film boundary layer. Tables 3–6 give a breakdown of the calculated values of the respective parameters of the first-order kinetic model. Based on the experimental and calculated values, it can be concluded that the adsorption of MG on ZnS-NP-AC is not probably following the pseudo-first-order kinetic model.

3.7.2. Pseudo-second-order kinetic model

Adsorption process with chemisorptions being the rate-control follows the pseudo-second-order model [29–32]. The sorption kinetics may be represented by the pseudo-second-order model as follows:

$$\frac{dq_t}{dt} = k_2(q_e - q_t)^2 \tag{19}$$

where k_2 is the equilibrium rate constant for the pseudo-second-order sorption (g mg^{-1} min^{-1}). The rate law for a pseudo-first-order reaction results in Eq. (19) after integrating and rearranging Eq. (20):

$$\frac{t}{q_t} = \frac{1}{k_2 q_e^2} + \frac{t}{q_e} \tag{20}$$

The plot of t/q_t vs. t gives a straight line with a slope of $1/q_e$ and intercept of $1/(k_2 q_e^2)$; these parameters were calculated from the slope. Tables 3–6 show the values determined from the intercept and their values in addition to corresponding regression coefficient (R^2) values. From the value of regression coefficients (close to

Table 3
Kinetic parameters of MG adsorption onto ZnS-NP-AC under conditions: 0.005 g of the adsorbent over 5–30 mg L^{-1} at pH 7, 0.5–35 min contact time and room temperature

Parameter values: concentration dye (ppm)							
Models	Parameters	5	10	15	20	25	30
First-order kinetic model:	k_1	0.0852	0.0736	0.0391	0.0184	0.0207	0.0184
$\log(q_e - q_t) = \log(q_e) - (k_1/2.303)t$	$q_{e,cal}$	65.162	150.314	208.449	248.885	326.587	400.866
	R^2	0.982	0.944	0.944	0.986	0.990	0.942
Second-order kinetic model:	k_2	0.003	0.0008	0.00056	0.0011	0.00044	0.00044
$t/q_t = 1/k_2q_e^2 + (1/q_e)t$	$q_{e,cal}$	111.111	250	333.3	333.3	500	500
	R^2	0.990	0.967	0.953	0.978	0.970	0.949
	H	37.03	50	62.5	111.111	111.111	111.111
Intraparticle diffusion: $q_t = K_{id}t^{1/2} + C$	K_{dif}	11.24	23.13	28.15	24.47	33.51	35.39
	C	34.05	53.75	74.43	117.9	127.9	151.8
	R^2	0.991	0.981	0.963	0.980	0.970	0.902
Elovich: $q_t = 1/\beta \ln(\alpha\beta) + 1/\beta \ln(t)$	β	0.0707	0.0353	0.0294	0.0332	0.0246	0.0239
	R^2	0.947	0.865	0.829	0.874	0.838	0.737
Experimental data	$q_{e,exp}$	99.74	199.5	297.28	390.96	486.3	581.92

Table 4
Kinetic parameters of MG adsorption onto ZnS-NP-AC, under the following conditions: 0.01 g adsorbent over 5–30 mg L^{-1} at pH 7, 0.5–35 min contact time and room temperature

Parameter values: concentration dye (ppm)							
Models	Parameters	5	10	15	20	25	30
First-order kinetic model:	k_1	0.0990	0.0852	0.0414	0.0207	0.0207	0.0184
$\log(q_e - q_t) = \log(q_e) - (k_1/2.303)t$	$q_{e,cal}$	33.036	73.620	102.093	123.310	161.064	169.433
	R^2	0.986	0.947	0.946	0.979	0.981	0.936
Second-order kinetic model:	k_2	0.0072	0.00026	0.00158	0.00257	0.00138	0.00138
$t/q_t = 1/k_2q_e^2 + (1/q_e)t$	$q_{e,cal}$	52.63	111.111	142.85	142.85	200	200
	R^2	0.992	0.978	0.954	0.975	0.969	0.949
	H	20	29.41	32.25	52.63	55.55	55.55
Intraparticle diffusion:	K_{dif}	5.652	11.37	13.89	12.15	16.27	17.49
$q_t = K_{id}t^{1/2} + C$	C	18.01	30.99	40.56	60.91	68.08	77.84
	R^2	0.986	0.991	0.956	0.969	0.954	0.892
Elovich:	β	0.1381	0.0709	0.0599	0.0675	0.0701	0.0488
$q_t = 1/\beta \ln(\alpha\beta) + 1/\beta \ln(t)$	R^2	0.953	0.896	0.811	0.849	0.931	0.720
Experimental data	$q_{e,exp}$	49.91	99.84	148.72	195.69	243.53	291.09

unity), it is confirmed that the sorption kinetics of MG follows a pseudo-second-order process. As can be seen in Tables 3–6, the calculated values are those attained experimentally. The bottom line is that the adsorption of MG on ZnS-NP-AC can better be explained by the pseudo-second-order kinetic model in comparison with the first-order kinetic model. Also, the process is chemisorptions controlled.

Hence, to calculate the initial sorption rate (h) (Eq. (21)), the second-order rate constants were used; the values have been shown in Tables 3–6.

$$h = k_2q_e^2 \quad (21)$$

3.7.3. Intraparticle diffusion model

In the intraparticle diffusion model [26,35], it is assumed that the mechanism of dye adsorption on a sorbent material takes place by four phases: (a) migration of dye molecules from the bulk solution to adsorbent surface through the bulk diffusion; (b) diffusion of dye molecules by the boundary layer to the adsorbent's surface by film diffusion; (c) the transport of the dye molecules from the surface to the interior pores of the particle occurs through the following mechanisms: intraparticle diffusion or pore diffusion and (d) dye adsorption at an active site on the surface of material through chemical reaction by ion-exchange, complexation and/or chelation. Generally,

Table 5
Kinetic parameters of MG adsorption onto ZnS-NP-AC, under the following conditions: 0.015 g adsorbent over 5–30 mg L^{-1} at pH 7, 0.5–35 min contact time and room temperature

Parameter values: concentration dye (ppm)							
Models	Parameters	5	10	15	20	25	30
First-order kinetic model:	k_1	0.1128	0.0898	0.0460	0.0207	0.0207	0.0184
$\log(q_e - q_t) = \log(q_e) - (k_1/2.303)t$	$q_{e,cal}$	23.878	49.659	66.834	81.096	105.925	131.219
	R^2	0.963	0.937	0.938	0.976	0.975	0.916
Second-order kinetic model:	k_2	0.0104	0.00399	0.00288	0.00357	0.00236	0.00181
$t/q_t = 1/k_2q_e^2 + (1/q_e)t$	$q_{e,cal}$	35.71	71.42	90.90	100	125	142.85
	R^2	0.992	0.980	0.962	0.975	0.968	0.945
	H	13.33	20.40	23.80	35.71	37.03	37.03
Intraparticle diffusion:	K_{dif}	3.784	7.523	9.437	7.943	10.63	11.34
$q_t = K_{id}t^{1/2} + C$	C	12.17	21.56	29.21	42.18	47.29	54.46
	R^2	0.987	0.992	0.967	0.962	0.942	0.865
Elovich:	β	0.2062	0.1071	0.0877	0.1039	0.0701	0.0761
$q_t = 1/\beta \ln(\alpha\beta) + 1/\beta \ln(t)$	R^2	0.955	0.900	0.832	0.832	0.931	0.683
Experimental data	$q_{e,exp}$	33.306	66.586	99.34	130.553	162.433	194.253

Table 6
Kinetic parameters of MG adsorption onto ZnS-NP-AC, under the following conditions: 0.02 g adsorbent over 5–30 mg L^{-1} at pH 7, 0.5–35 min contact time and room temperature

Parameter values: concentration dye (ppm)							
Models	Parameters	5	10	15	20	25	30
First-order kinetic model:	k_1	0.1289	0.0967	0.0483	0.0230	0.0207	0.0184
$\log(q_e - q_t) = \log(q_e) - (k_1/2.303)t$	$q_{e,cal}$	20.090	38.370	49.545	61.376	77.803	96.161
	R^2	0.903	0.916	0.930	0.949	0.970	0.888
Second-order kinetic model:	k_2	0.0148	0.00546	0.00362	0.00422	0.00345	0.00285
$t/q_t = 1/k_2q_e^2 + (1/q_e)t$	$q_{e,cal}$	26.31	52.63	71.42	76.92	90.90	100
	R^2	0.992	0.976	0.963	0.968	0.968	0.944
	H	10.30	15.15	18.51	25	28.57	28.57
Intraparticle diffusion:	K_{dif}	2.833	5.539	7.033	6.297	7.806	8.054
$q_t = K_{id}t^{1/2} + C$	C	9.310	16.77	22.90	31.52	37.64	43.82
	R^2	0.986	0.983	0.967	0.943	0.936	0.828
Elovich:	β	0.2751	0.1462	0.1173	0.1319	0.0701	0.1085
$q_t = 1/\beta \ln(\alpha\beta) + 1/\beta \ln(t)$	R^2	0.956	0.883	0.836	0.806	0.931	0.639
Experimental data	$q_{e,exp}$	24.995	49.955	74.565	98.11	121.995	145.865

both the liquid phase mass transport rate and the intraparticle mass transport rate control the sorption of MG. In order to take into account both the particle size and particle shape, pore-diffusion models should be formulated. Since the rate can be described in regard to the square root of time (t), the adsorption is a diffusive mass transfer process. Eq. (22) describes the intraparticle diffusion model as [28–31,35,46]:

$$q_t = k_i t^{0.5} + C \tag{22}$$

where q_t is the fraction dye uptake (mg g^{-1}) at time t, k_i is the intraparticle diffusion rate constant (mg g^{-1} min^{-1}) and C is the intercept (mg g^{-1}). The plot of q_t vs. t^{05} gives k_i as slope and C as intercept. The intercept represents the effect of boundary layer thickness. The minimum is the intercept length and adsorption is less boundary layer controlled. Tables 3–6 show a summary of k_i and C values and the regression constant (R^2) as well. The gained straight line illustrates that the dye molecules are transported to the external surface of the adsorbent through film diffusion, and its rate is very quick. The intraparticle diffusion is not the only rate limiting mechanism since the line did not pass through the origin. Therefore, it can be said that MG adsorption onto ZnS-NP-AC is a complicated process, and both intraparticle diffusion and surface sorption (film diffusion) contribute to the rate-limiting step.

3.7.4. Elovich equation

In this model with known Eq. (23):

$$q_t = 1/\beta \ln(\alpha\beta) + 1/\beta \ln(t) \quad (23)$$

where α is the initial adsorption rate (mg g^{-1} min^{-1}), and β is the desorption constant related to the extent of surface coverage and activation energy for chemisorption (g mg^{-1}). The parameters (1/β) and (1/β)ln(αβ) can be calculated from the slope and intercept of the linear plot of q_t vs. ln(t). The obtained R^2 values of this model were <0.8900 for MG initial concentration in the range of 5–30 mg L^{-1} on ZnS-NP-AC adsorbent (Tables 3–6). The parameter 1/β is related to the number of sites available for adsorption while (1/β)ln(αβ) is the adsorption quantity when ln$t$ is equal to zero. In order to reach a better understanding on the adsorption behavior of the first step, the adsorption quantity at 1 min is useful [47–50].

3.8. MLR model

In this work, the MLR model was utilized to know that there is a linear relationship existing between normalized inputs and normalized removal (%). The MLR model for training set was achieved by means of three inputs, and the following equation was achieved:

$$Y = 0.516 - 0.610x_1 + 0.367x_2 + 0.126x_3 \quad (24)$$

where Y, x_1, x_2 and x_3 are the removal (%), dye content (mg L^{-1}), contact time (min) and adsorbent dosage (g), respectively. Then, the model was employed for removal forecasting of the testing set. Fig. 12(a) exhibits the predicted values of normalized removal of data in the training, and testing sets using the MLR model and their plotting against normalized experimental data. The statistical findings of the MLR model display a coefficient of determination (R^2) of 0.9134 and MSE of 0.0038 for the training set. Further, the model was considered on the testing set: the result presents R^2 = 0.9091 and MSE = 0.0038.

3.9. RF model

RF has three tuning parameters, including n_{tree}, m_{try} and extra_options. Table 7 demonstrates the range tuning parameters and gained coefficient of determination (R^2) and MSE for the training set and testing set. Based on the results, the optimal tuning parameters for the RF model are attained according to the n_{tree} = 100, m_{try} = 2, importance = 1 and nPerm = 3 (nPerm indicates the number of times the OOB data are changed per tree for studying variable importance) in the forest. In optimal model, for the training and testing sets, the MSE values of 0.0002 and 0.0007 and the R^2 values of 0.9951 and 0.9826 are achieved, respectively. Fig. 12(b) shows the performance of the optimal RF model for the data sets. The OOB error rate against some trees is plotted (Fig. 12(c)). It can be seen that the OOB error rate converges at a point after 200 trees and stays unchanged

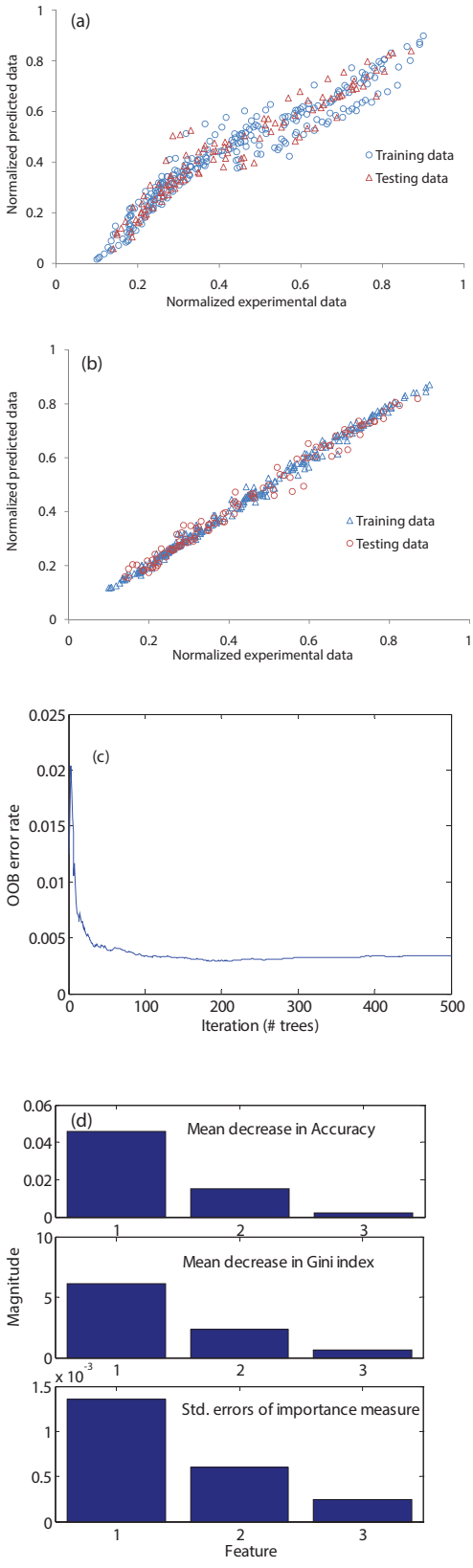

Fig. 12. The experimental data against the predicted data of normalized removal obtained with (a) MLR, (b) RF models, (c) the OOB error rate against number of trees and (d) the importance of each variable.

Table 7
The range of tuning parameters and achieved statistical data for training and testing data sets

	n_{tree}	m_{try}	Extra_options	Training set		Testing set	
				R^2	MSE	R^2	MSE
1	500	1	–	0.9457	0.0024	0.9228	0.0031
2	100	1	–	0.9581	0.0018	0.9379	0.0025
3	100	2	–	0.9943	2.5e–04	0.9796	8.3e–04
4[a]	500	1	–	0.9548	0.0020	0.9323	0.0027
5[b]	100	4	Without replacement	0.9329	0.0029	0.9023	0.0040
6	100	4	sampsize = size(X_trn,1)*2/3	0.9339	0.0029	0.9076	0.0037
7[c]	100	4	nodesize = 7	0.9439	0.0024	0.9235	0.0031
8[d]	100	4	importance = 1	0.9467	0.0023	0.9176	0.0033
9[d]	100	4	localImp = 1	0.9481	0.0023	0.9206	0.0032
10[d]	100	4	proximity = 1	0.9459	0.0024	0.9125	0.0035
11[e]	100	4	proximity = 1; oob_prox = 0	0.9500	0.0022	0.9277	0.0029
12[d]	100	4	do_trace = 1	0.9580	0.0018	0.9335	0.0026
13[d]	100	4	In-bag = 1	0.9547	0.0020	0.9317	0.0028
14[d]	100	2	importance = 1; nPerm = 1	0.9445	0.0024	0.9217	0.0032
15	100	2	importance = 1; nPerm = 3	0.9951	2.1e–04	0.9826	7.1e–04

[a]Set to default trees and m_{try} by specifying values as 0.
[b]Set sampling without replacement (default is with replacement).
[c]Note that the default value is 5 for regression.
[d]Default (Don't) = 0.
[e]Default = 1 if proximity is enabled, Don't 0.

and increasing more trees does not decrease the OOB error rate. The importance of each variable can be shown by a mean decrease in Gini index and a mean decrease in accuracy. The mean decrease in accuracy of the variable is estimated in the OOB error computation. Variables having a great mean decline in accuracy are more important among the data. The homogeneity of the nodes and leaves in the resulting RF for each variable can be determined by the mean decrease in Gini index. Variables with a large mean decrease in Gini index have higher purity (Fig. 12(d)). By comparing the results of the models, we can see that there is a good agreement between the predicted data and the experimental data, while the RF model is better than the MLR model (Table 8).

Table 8
Comparison of MSE and R^2 values obtained by the MLR and RF models

Model	Training set		Testing set	
	MSE	R^2	MSE	R^2
RF	2.1e–04	0.9951	7.1e–04	0.9826
MLR	0.0038	0.9134	0.008	0.9091

3.10. Comparison with other adsorbents for malachite green dye

Several previous studies have reported many adsorbents for MG adsorption [12,29,51–62] and investigated these adsorbents in terms of costs and contact times. Table 9 compares the adsorption capacity, contact time and adsorbent dose of a few adsorbents. As can be clearly seen, as compared with other studies, the adsorbent used in the current work had the highest adsorption capacity and needed shorter required time and dosage [29].

4. Conclusion

Zinc sulfide-based nanoparticle was synthesized and characterized, and subsequently loaded onto activated carbon and used for MG removal from the aqueous medium. BET, FESEM, BJH, UV spectrum and XRD techniques were used for characterization of the adsorbent. Also, the impacts of various operating parameters such as solution pH, adsorbent dosage, initial dye concentration and contact time on the extent of dye adsorption were investigated. ZnS-NP-AC was found to be a beneficial adsorbent for MG removal from aqueous environments and, more importantly, its equilibrium time is <20 min. Kinetics of adsorption was found to follow the Langmuir isotherms best represented as a second-order rate expression and adsorption equilibrium data for the adsorbent. ZnS-NP-AC was capable of removing 98% of MG only in 15 min. The highest adsorption capacity of ZnS-NP-AC was 500 mg g^{-1}, which was by far higher than those of adsorbents that have recently been used. Moreover, we used an RF model as a beneficial tool to project the removal efficiency of MG from aqueous solutions via zinc sulfide nanoparticle loaded with activated carbon. The results illustrated that experimental data are well consistent with the simulated data with the RF model.

Table 9
Comparison of adsorption capacities, contact time and adsorbent dose for the MG removal

Adsorbent	Adsorption capacity (mg g^{-1})	Contact time	Adsorbent dose	Source
Arundo donax root carbon	8.7	180 min	0.15–1.0 g	[61]
Lemon peel	3.2–51.7	24 h	0.05 g	[12]
Cyclodextrin-based material	91.9	120 min	0.15 g	[55]
Rice husk	76.9	60 min	0.6 g	[54]
Oil palm trunk fiber	149.4	120 min	–	[60]
Chitosan bead	93.6	300 min		[59]
Activated charcoal	0.18	30 min	0.01 g	[56]
Neem sawdust	4.4	14 min	2.517 g	[62]
ZnO-NP-AC	322.6	0.5–30 min	0.005 g	[29]
ZnS-NP-AC	500.0	0.5–35 min	0.005 g	This study

Symbols

C_t	—	Dye concentration at time t, mg L^{-1}
V	—	Volume of solution, L
W	—	Weight of adsorbent, g
Q_e	—	Equilibrium adsorption capacity, mg g^{-1}
C_e	—	Dye concentration at equilibrium, mg L^{-1}
H	—	Second-order rate constants, mg g^{-1} min^{-1}
α	—	Initial adsorption rate, mg g^{-1} min^{-1}
k_1	—	Rate constant of pseudo-first-order adsorption, min^{-1}
k_2	—	Second-order rate constant of adsorption, mg g^{-1} min^{-1}
K_{dif}	—	Rate constant of intraparticle diffusion, mg g^{-1} $min^{-1/2}$
F	—	Fraction of solute adsorbed at any time t, mg g^{-1}
β	—	Desorption constant, mg g^{-1}
C	—	Intercept of intraparticle diffusion (related to the thickness of the boundary layer)
D_i	—	Effective diffusion coefficient of adsorbate in adsorbent phase
r^2	—	Radius of adsorbent particles, m
Q_m	—	Maximum adsorption capacity reflected a complete monolayer in Langmuir isotherm model, mg g^{-1}
K_a	—	Langmuir constant or adsorption equilibrium constant that is related to the apparent energy of sorption, L mg^{-1}
RL	—	Dimensionless equilibrium parameter (separation factor)
K_f	—	Isotherm constant indicates the capacity parameter related to the intensity of the adsorption, mg g^{-1}
N	—	Isotherm constant indicates the empirical parameter related to the intensity of the adsorption, g L^{-1}
T	—	Absolute temperature, K
R	—	Universal gas constant, 8.314 J K^{-1} mol^{-1}
B_1	—	Related to the heat of adsorption ($B_1 = RT/b$)
b_T	—	Constant related to the heat of adsorption
K_T	—	Equilibrium binding constant
K	—	Constant related to the adsorption energy at the D–R isotherm, mol^2 kJ^{-2}
Q_m	—	Theoretical saturation capacity at the D–R isotherm
ε	—	Polanyi potential at the D–R isotherm
E	—	Mean free energy of adsorption
X^2	—	Chi-squared test statistic
$q_{e,exp}$	—	Experimental data of the equilibrium capacity, mg g^{-1}
$q_{e,cal}$	—	Equilibrium capacity obtained by calculating from the isotherm model, mg g^{-1}
R^2	—	Correlation coefficient

References

[1] M. Ghaedi, F.N. Azad, K. Dashtian, S. Hajati, A. Goudarzi, M. Soylak, Central composite design and genetic algorithm applied for the optimization of ultrasonic-assisted removal of malachite green by ZnO nanorod-loaded activated carbon, Spectrochim. Acta, Part A, 167 (2016) 157–164.

[2] A.R. Rahmani, K. Godini, D. Nematollahi, G. Azarian, S. Maleki, Degradation of azo dye CI Acid Red 18 using an eco-friendly and continuous electrochemical process, Korean J. Chem. Eng., 33 (2016) 532–538.

[3] F. Zhang, B. Ma, X. Jiang, Y. Ji, Dual function magnetic hydroxyapatite nanopowder for removal of malachite green and Congo red from aqueous solution, Powder Technol., 302 (2016) 207–214.

[4] E.A. Dil, M. Ghaedi, A. Asfaram, S. Hajati, F. Mehrabi, A. Goudarzi, Preparation of nanomaterials for the ultrasound-enhanced removal of Pb^{2+} ions and malachite green dye: chemometric optimization and modeling, Ultrason. Sonochem., 34 (2017) 677–691.

[5] Y.J. Chang, C. Munsee, G. Herman, J. Wager, P. Mugdur, D.H. Lee, C.H. Chang, Growth, characterization and application of CdS thin films deposited by chemical bath deposition, Surf. Interface Anal., 37 (2005) 398–405.

[6] M. Rajabi, B. Mirza, K. Mahanpoor, M. Mirjalili, F. Najafi, O. Moradi, H. Sadegh, R. Shahryari-ghoshekandi, M. Asif, I. Tyagi, Adsorption of malachite green from aqueous solution by carboxylate group functionalized multi-walled carbon nanotubes: determination of equilibrium and kinetics parameters, J. Ind. Eng. Chem., 34 (2016) 130–138.

[7] P. Brown, I.A. Jefcoat, D. Parrish, S. Gill, E. Graham, Evaluation of the adsorptive capacity of peanut hull pellets for heavy metals in solution, Adv. Environ. Res., 4 (2000) 19–29.

[8] A. Goudarzi, G.M. Aval, S.S. Park, M.-C. Choi, R. Sahraei, M.H. Ullah, A. Avane, C.-S. Ha, Low-temperature growth of nanocrystalline Mn-doped ZnS thin films prepared by chemical bath deposition and optical properties, Chem. Mater., 21 (2009) 2375–2385.

[9] K. Singh, M. Talat, S. Hasan, Removal of lead from aqueous solutions by agricultural waste maize bran, Bioresour. Technol., 97 (2006) 2124–2130.
[10] P. Assefi, M. Ghaedi, A. Ansari, M. Habibi, M. Momeni, Artificial neural network optimization for removal of hazardous dye Eosin Y from aqueous solution using Co_2O_3-NP-AC: isotherm and kinetics study, J. Ind. Eng. Chem., 20 (2014) 2905–2913.
[11] Z. Reddad, C. Gerente, Y. Andres, P. Le Cloirec, Adsorption of several metal ions onto a low-cost biosorbent: kinetic and equilibrium studies, Environ. Sci. Technol., 36 (2002) 2067–2073.
[12] K.V. Kumar, Optimum sorption isotherm by linear and non-linear methods for malachite green onto lemon peel, Dyes Pigm., 74 (2007) 595–597.
[13] R. Gong, X. Zhang, H. Liu, Y. Sun, B. Liu, Uptake of cationic dyes from aqueous solution by biosorption onto granular kohlrabi peel, Bioresour. Technol., 98 (2007) 1319–1323.
[14] M. Husseien, A. Amer, A. El-Maghraby, N.A. Taha, Utilization of barley straw as a source of a activated carbon for removal of methylene blue from aqueous solution, J. Appl. Sci. Res., 3 (2007) 1352–1358.
[15] N. Pramanpol, N. Nitayapat, Adsorption of reactive dye by eggshell and its membrane, Kasetsart J., 40 (2006) 192–197.
[16] W.-T. Tsai, H.-R. Chen, K.-C. Kuo, C.-Y. Lai, T.-C. Su, Y.-M. Chang, J.-M. Yang, The adsorption of methylene blue from aqueous solution using waste aquacultural shell powders, J. Environ. Eng. Manage., 19 (2009) 165–172.
[17] M. Qiu, C. Qian, J. Xu, J. Wu, G. Wang, Studies on the adsorption of dyes into clinoptilolite, Desalination, 243 (2009) 286–292.
[18] M. Ghaedi, H. Hossainian, M. Montazerozohori, A. Shokrollahi, F. Shojaipour, M. Soylak, M. Purkait, A novel acorn based adsorbent for the removal of brilliant green, Desalination, 281 (2011) 226–233.
[19] E. Lorenc-Grabowska, G. Gryglewicz, Adsorption characteristics of Congo Red on coal-based mesoporous activated carbon, Dyes Pigm., 74 (2007) 34–40.
[20] L. Lian, L. Guo, A. Wang, Use of $CaCl_2$ modified bentonite for removal of Congo red dye from aqueous solutions, Desalination, 249 (2009) 797–801.
[21] S. Arellano-Cárdenas, S. López-Cortez, M. Cornejo-Mazón, J.C. Mares-Gutiérrez, Study of malachite green adsorption by organically modified clay using a batch method, Appl. Surf. Sci., 280 (2013) 74–78.
[22] P.A. Belter, E.L. Cussler, W. Hu, A Review of Bioseparations, (Downstream Processing for Biotechnology), Wiley Interscience, New York, 1988.
[23] S. Curteanu, K. Godini, C.G. Piuleac, G. Azarian, A.R. Rahmani, C. Butnariu, Electro-oxidation method applied for activated sludge treatment: experiment and simulation based on supervised machine learning methods, Ind. Eng. Chem. Res., 53 (2014) 4902–4912.
[24] M. Ghaedi, A. Ghaedi, E. Negintaji, A. Ansari, F. Mohammadi, Artificial neural network – imperialist competitive algorithm based optimization for removal of sunset yellow using $Zn(OH)_2$ nanoparticles-activated carbon, J. Ind. Eng. Chem., 20 (2014) 4332–4343.
[25] M. Ghaedi, A. Ansari, P. Assefi Nejad, A. Ghaedi, A. Vafaei, M.H. Habibi, Artificial neural network and Bees Algorithm for removal of Eosin B using cobalt oxide nanoparticle-activated carbon: isotherm and kinetics study, Environ. Prog. Sustain. Energy, 34 (2015) 155–168.
[26] M. Ghaedi, A. Ghaedi, M. Hossainpour, A. Ansari, M. Habibi, A. Asghari, Least square-support vector (LS-SVM) method for modeling of methylene blue dye adsorption using copper oxide loaded on activated carbon: kinetic and isotherm study, J. Ind. Eng. Chem., 20 (2014) 1641–1649.
[27] A.E. Raevskaya, A.V. Korzhak, A.L. Stroyuk, S.Y. Kuchmii, Spectro-optical and photochemical properties of ZnS nanoparticles, Theor. Exp. Chem., 41 (2005) 111–116.
[28] M. Ghaedi, A. Ansari, R. Sahraei, ZnS:Cu nanoparticles loaded on activated carbon as novel adsorbent for kinetic, thermodynamic and isotherm studies of Reactive Orange 12 and Direct yellow 12 adsorption, Spectrochim. Acta, Part A, 114 (2013) 687–694.
[29] M. Ghaedi, A. Ansari, M. Habibi, A. Asghari, Removal of malachite green from aqueous solution by zinc oxide nanoparticle loaded on activated carbon: kinetics and isotherm study, J. Ind. Eng. Chem., 20 (2014) 17–28.
[30] S. Alizadeh, D. Nematollahi, Electrochemically Assisted self-assembly technique for the fabrication of mesoporous metal–organic framework thin films: composition of 3D hexagonally packed crystals with 2D honeycomb-like mesopores, J. Am. Chem. Soc., 139 (2017) 4753–4761.
[31] M. Ravanan, M. Ghaedi, A. Ansari, F. Taghizadeh, D. Elhamifar, Comparison of the efficiency of Cu and silver nanoparticle loaded on supports for the removal of Eosin Y from aqueous solution: kinetic and isotherm study, Spectrochim. Acta, Part A, 123 (2014) 467–472.
[32] M. Ghaedi, A.M. Ghaedi, A. Ansari, F. Mohammadi, A. Vafaei, Artificial neural network and particle swarm optimization for removal of methyl orange by gold nanoparticles loaded on activated carbon and Tamarisk, Spectrochim. Acta, Part A, 132 (2014) 639–654.
[33] A. Shamsizadeh, M. Ghaedi, A. Ansari, S. Azizian, M. Purkait, Tin oxide nanoparticle loaded on activated carbon as new adsorbent for efficient removal of malachite green-oxalate: non-linear kinetics and isotherm study, J. Mol. Liq., 195 (2014) 212–218.
[34] K. Ahmadi, M. Ghaedi, A. Ansari, Comparison of nickel doped zinc sulfide and/or palladium nanoparticle loaded on activated carbon as efficient adsorbents for kinetic and equilibrium study of removal of Congo Red dye, Spectrochim. Acta, Part A, 136 (2015) 1441–1449.
[35] M. Ghaedi, A.M. Ghaedi, E. Negintaji, A. Ansari, A. Vafaei, M. Rajabi, Random forest model for removal of bromophenol blue using activated carbon obtained from *Astragalus bisulcatus* tree, J. Ind. Eng. Chem., 20 (2014) 1793–1803.
[36] M. Hadi, M.R. Samarghandi, G. McKay, Equilibrium two-parameter isotherms of acid dyes sorption by activated carbons: study of residual errors, Chem. Eng. J., 160 (2010) 408–416.
[37] I. Langmuir, The adsorption of gases on plane surfaces of glass, mica and platinum, J. Am. Chem. Soc., 40 (1918) 1361–1403.
[38] H. Freundlich, Over the adsorption in solution, J. Phys. Chem., 57 (1906) 1100–1107.
[39] M. Temkin, V. Pyzhev, Recent modifications to Langmuir isotherms, Acta Physiochim URSS, 12 (1940) 217–222.
[40] X.-s. Wang, Y. Qin, Equilibrium sorption isotherms for of Cu^{2+} on rice bran, Process Biochem., 40 (2005) 677–680.
[41] M. Dubinin, The potential theory of adsorption of gases and vapors for adsorbents with energetically nonuniform surfaces, Chem. Rev., 60 (1960) 235–241.
[42] M. Dubinin, Modern state of the theory of volume filling of micropore adsorbents during adsorption of gases and steams on carbon adsorbents, Zh. Fiz. Khim., 39 (1965) 1305–1317.
[43] L. Radushkevich, Potential theory of sorption and structure of carbons, Zh. Fiz. Khim., 23 (1949) 1410–1420.
[44] Y.-S. Ho, A.E. Ofomaja, Kinetics and thermodynamics of lead ion sorption on palm kernel fibre from aqueous solution, Process Biochem., 40 (2005) 3455–3461.
[45] G. Asgari, B. Roshani, G. Ghanizadeh, The investigation of kinetic and isotherm of fluoride adsorption onto functionalize pumice stone, J. Hazard. Mater., 217 (2012) 123–132.
[46] L. Breiman, Random forests, Mach. Learn., 45 (2001) 5–32.
[47] Y.-S. Ho, Second-order kinetic model for the sorption of cadmium onto tree fern: a comparison of linear and non-linear methods, Water Res., 40 (2006) 119–125.
[48] R.-L. Tseng, Mesopore control of high surface area NaOH-activated carbon, J. Colloid Interface Sci., 303 (2006) 494–502.
[49] K. Li, X. Wang, Adsorptive removal of Pb(II) by activated carbon prepared from *Spartina alterniflora*: equilibrium, kinetics and thermodynamics, Bioresour. Technol., 100 (2009) 2810–2815.
[50] S. Chen, J. Zhang, C. Zhang, Q. Yue, Y. Li, C. Li, Equilibrium and kinetic studies of methyl orange and methyl violet adsorption on activated carbon derived from *Phragmites australis*, Desalination, 252 (2010) 149–156.

[51] V.K. Gupta, S.K. Srivastava, D. Mohan, Equilibrium uptake, sorption dynamics, process optimization, and column operations for the removal and recovery of malachite green from wastewater using activated carbon and activated slag, Ind. Eng. Chem. Res., 36 (1997) 2207–2218.
[52] V. Garg, R. Gupta, A.B. Yadav, R. Kumar, Dye removal from aqueous solution by adsorption on treated sawdust, Bioresour. Technol., 89 (2003) 121–124.
[53] C. Akmil-Başar, Y. Önal, T. Kılıçer, D. Eren, Adsorptions of high concentration malachite green by two activated carbons having different porous structures, J. Hazard. Mater., 127 (2005) 73–80.
[54] I. Rahman, B. Saad, S. Shaidan, E.S. Rizal, Adsorption characteristics of malachite green on activated carbon derived from rice husks produced by chemical–thermal process, Bioresour. Technol., 96 (2005) 1578–1583.
[55] G. Crini, H.N. Peindy, F. Gimbert, C. Robert, Removal of CI Basic Green 4 (Malachite Green) from aqueous solutions by adsorption using cyclodextrin-based adsorbent: kinetic and equilibrium studies, Sep. Purif. Technol., 53 (2007) 97–110.
[56] M.J. Iqbal, M.N. Ashiq, Adsorption of dyes from aqueous solutions on activated charcoal, J. Hazard. Mater., 139 (2007) 57–66.
[57] R. Malik, D. Ramteke, S. Wate, Adsorption of malachite green on groundnut shell waste based powdered activated carbon, Waste Manage., 27 (2007) 1129–1138.
[58] Y. Önal, C. Akmil-Başar, Ç. Sarıcı-Özdemir, Investigation kinetics mechanisms of adsorption malachite green onto activated carbon, J. Hazard. Mater., 146 (2007) 194–203.
[59] Z. Bekçi, C. Özveri, Y. Seki, K. Yurdakoç, Sorption of malachite green on chitosan bead, J. Hazard. Mater., 154 (2008) 254–261.
[60] B. Hameed, M. El-Khaiary, Batch removal of malachite green from aqueous solutions by adsorption on oil palm trunk fibre: equilibrium isotherms and kinetic studies, J. Hazard. Mater., 154 (2008) 237–244.
[61] J. Zhang, Y. Li, C. Zhang, Y. Jing, Adsorption of malachite green from aqueous solution onto carbon prepared from *Arundo donax* root, J. Hazard. Mater., 150 (2008) 774–782.
[62] S. Khattri, M. Singh, Removal of malachite green from dye wastewater using neem sawdust by adsorption, J. Hazard. Mater., 167 (2009) 1089–1094.